Assembly of $CuIn_{1-x}Ga_xS_2$ Nanorods into Highly Ordered 2D and 3D Superstructures

Ajay Singh,[†,‡] Claudia Coughlan,[†,‡] Fathima Laffir,[†] and Kevin M. Ryan[†,‡,*]

[†]Materials and Surface Science Institute and Department of Chemical and Environmental Sciences and [‡]SFI-Strategic Research Cluster in Solar Energy Research, University of Limerick, Limerick, Ireland

ABSTRACT

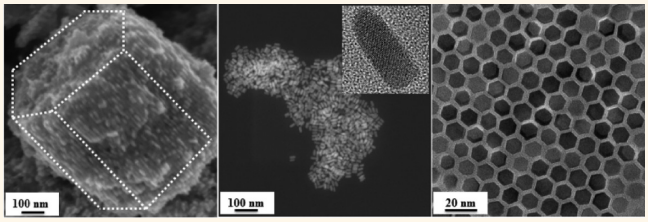

Here, we report self- and directed assembly of $CuIn_{1-x}Ga_xS_2$ (CIGS) nanorods into highly ordered 2D and 3D superstructures. The assembly protocol is dictated by the ligand environment and is hence chemically tunable. Thiol capped nanorods spontaneously assemble into 3D aligned nanorod clusters over a period of hours with end to end and side to side order. These clusters can be disassembled by ligand exchange with an amine and subsequently reassembled either at a substrate interface or as free floating 2D sheets by directed assembly protocols. This dimensional control of CIGS nanorod assembly, extending over device scale areas with high degrees of order, is highly attractive for applications utilizing these important quaternary photoabsorbers.

KEYWORDS: nanocrystal · nanorod · perpendicular assembly · CIGS · CIS · supra-crystal

Colloidal nanocrystal routes to the quaternary copper chalcogenide $CuIn_{1-x}Ga_xS_2$ (CIGS) offer attractive solution processing of this compound semiconductor.[1−6] Formation as a nanocrystal locks in the correct stoichiometry, a major challenge in coevaporation approaches where multiple phases occur particularly at grain boundaries.[7−9] The direct band gap varies with (In/Ga) composition and can be tuned from 1.5 to 2.4 eV by judicious selection of metal precursor ratios during synthesis.[3−5] The low toxicity, high radiation stability, and high absorption coefficients of CIGS nanocrystals allows for wide ranging applications in photocatalytic, thermoelectric, and photovoltaic devices.[1−6,10−12] In nanocrystals, the wurtzite phase of copper chalcogenides is stable allowing for ligand-assisted shape control with nanorod growth occurring along the (002) direction.[12−16] This geometry allows length-dependent properties such as total absorption and conductivity to be harnessed independent of diameter-dependent properties such as band gap.[17−19] Subsequent assembly allows for the possibility of large scale arrays with each nanorod vertically aligned and close packed thereby maximizing the collective properties in a densely packed superstructure.[18,20]

The progress in understanding and hence controlling nanorod assembly has led to approaches ranging from simple evaporation, through to external perturbation by additives (depletion attraction), highly oriented pyrolytic graphite (HOPG), or electric fields.[20−32] We have recently shown that Coulombic interactions owing to the net charge and dipole on the nanorods exert the largest influence on the type of assembly that occurs.[21−23] In ambient solutions, if the attractive interactions (dipole−dipole) outweigh the repulsive interactions (charge−charge) assembly will occur as a function of distance and hence concentration.[21−23] In solution, this constitutes as assembly into 2D monolayers which deposit to the surface at a specific concentration. Alternatively, under an electric field the net charge results in electrophoretic migration with axial orientation due to the dipole.[28] As the dipole is intrinsic to the wurtzite lattice and the charge can be modulated by a ligand, this gives a relatively facile approach to tailor the assembly formation as needed with up to centimeter scale areas reported.[28] With copper chalcogenides, assemblies of binary (Cu_2S) and ternary ($CuInS_2$) nanorods have been demonstrated by slow evaporation of solutions over relatively small areas, whereas Cu_2S nanoplates have been shown to spontaneously organize into 3D supercrystals within the solution phase.[16,33] We

* Address correspondence to kevin.m.ryan@ul.ie.

Received for review May 6, 2012 and accepted July 5, 2012.

Published online July 05, 2012
10.1021/nn301999b

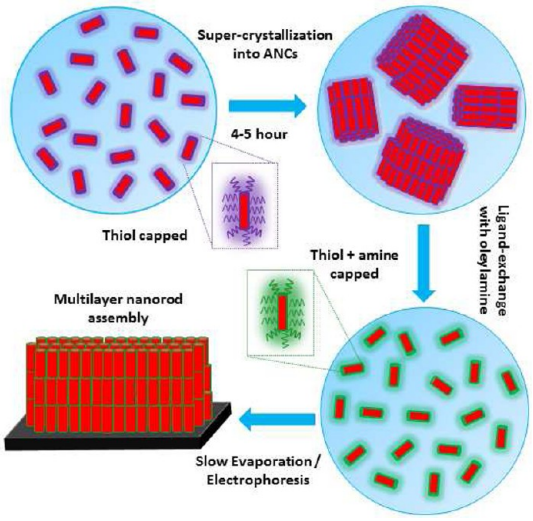

Figure 1. Schematic representation shows the assembly and deassembly of CIGS nanorods.

recently showed the synthesis and subsequent assembly of quaternary Cu_2ZnSnS_4 (CZTS) nanorods from solution using charge/dipole interactions.[15]

Here we show controllable assembly formation with the important $CuIn_{1-x}Ga_xS_2$ (CIGS) nanorods over two and three dimensions. The assembly was primarily enabled by a synthetic optimization to allow monodisperse nanorod formation (without L-shaped nanocrystals). The as-synthesized nanorods are thiol capped and over 4−5 h spontaneously self-assemble into highly ordered 3D nanocrystal clusters (Figure 1). We further show that we can deassemble these clusters by the facile introduction of an amine ligand; reverting the solution to a random nanorod dispersion.[34] As these nanorods have a modified ligand environment (thiol/amine) and net charge, their assembly can be controlled by either optimizing the solution concentration (to form free floating 2D sheets) or by electrophoresis. The subsequent formation of monolayer to multilayer assemblies of vertically aligned CIGS nanorods directly on substrates is therefore possible. This reversible assembly and disassembly protocol is extendable to a range of ternary and quaternary nanorods and creates a facile chemical process for modulating nanorod assembly over 2 and 3 dimensions in these important semiconductor materials.

RESULTS AND DISCUSSION

Highly monodisperse CIGS nanorods 11 ± 0.5 nm in width and 24 ± 1 nm (Figure 2a) were synthesized using a modification of procedure from Gupta et al.[14] (see experimental section). The nanorods are defect-free wurtzite single crystals (XRD inset Figure 2a) with elongation occurring along the [002] direction and with a *d*-spacing of 0.318 nm (TEM Figure 2b).

Spontaneous nanorod assembly occurs in a solution of these thiol capped nanorods when left for a period

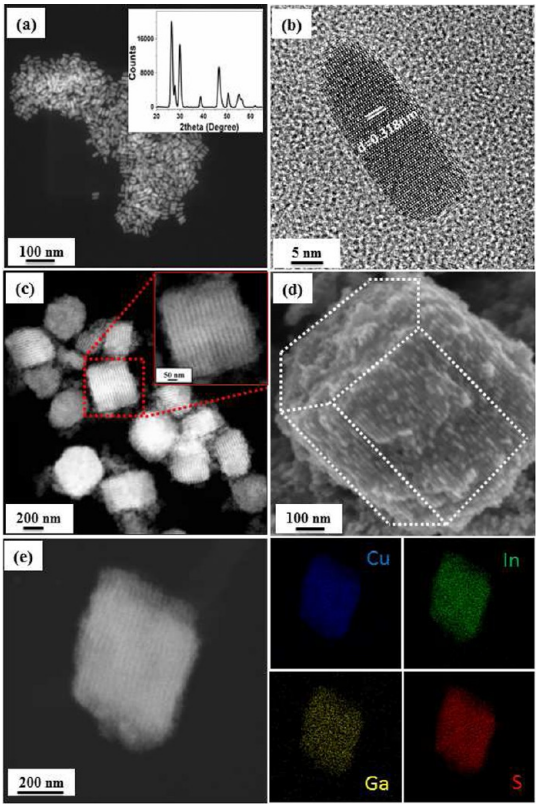

Figure 2. Low-resolution angular dark-field STEM (DF-STEM) of monodispersed CIGS nanorods with inset XRD pattern confirming their wurtzite structure. (b) HRTEM image of nanorod. (c) Low-resolution DF-STEM image showing the CIGS ANCs with inset high-resolution DF-STEM image. (d) HRSEM image shows the side-by-side alignment of nanorods in individual ANC. (e) HAADF STEM image of CIGS ANC with corresponding EDS elemental mapping images.

of 4−5 h resulting in submicrometer-sized aligned nanorod clusters (ANCs) consisting of close packed rods stacked end-to-end and side-by-side. The size of the clusters varies from 500 to 800 nm (Figure 2c). In Figure 2d, the hexagonal symmetry of the ANCs is evident suggesting that the nanorods prefer to adopt hexagonal close packed (hcp) packing arrangements to attain the highest packing efficiency and minimize the potential energy.[35−37] Elemental mapping of an ANC (Figure 2e) further confirms that Cu, In, Ga, and S are evenly distributed with chemical composition close to $CuIn_{0.75}Ga_{0.25}S_2$. The formation of ANCs in solution was further investigated by dynamic light scattering (DLS) showing an average hydrodynamic size at 500−800 nm (see Supporting Information, Figure S1) in good agreement with TEM and SEM data.

The degree of order and resolute close packing in these ANCs is highly attractive for applications where the collective properties of the nanorods can be exploited at a submicrometer length scale, for example, labeling, lighting, *etc.*[18−20] The ANCs show a broad UV−vis absorbance in comparison to well-dispersed

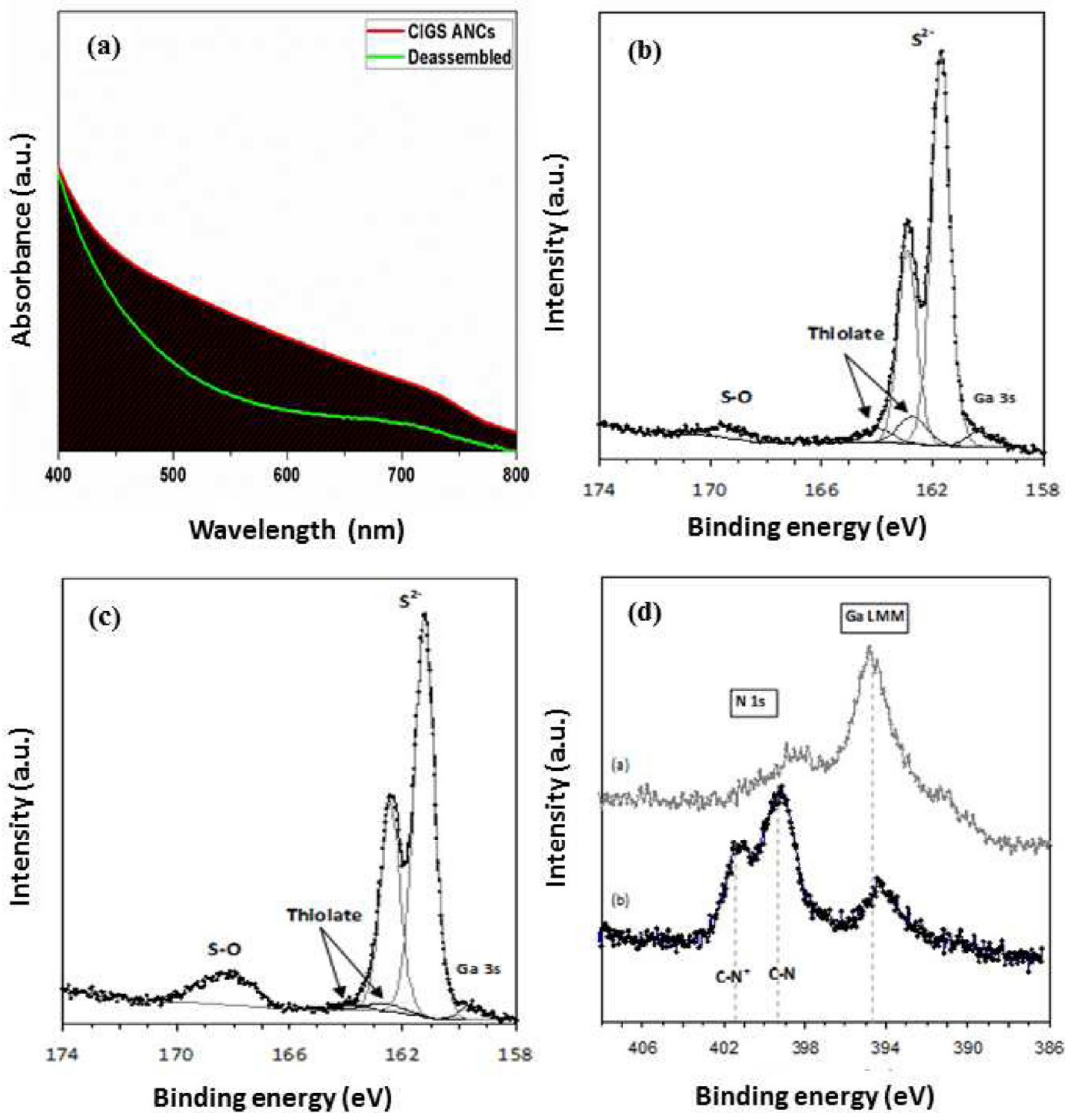

Figure 3. (a) UV−vis absorption spectra of CIGS ANCs (red) and after deassembly by oleylamine (green). (b−d) High-resolution XPS spectra of as-synthesized and ligand exchange CIGS nanorods.

nanorods as seen in Figure 3a (Supporting Information, Figure S2a). This can be attributed to increased dipole coupling between the nanorods in the closed packed arrangement when compared to the nonassembled nanorods. Similar behavior was recently reported for pseudo-spherical $Cu_{1.97}S$ nanocrystals.[34,38,39] The CIGS nanorods have a band gap of ~1.85 eV (Supporting Information, Figure S2b) determined by extrapolating the linear region of a plot of $(\alpha h\nu)^2$ *versus* energy, where α represent the absorption coefficient and $h\nu$ is photon energy, in good agreement with previous reports.[14]

While these ANCs can be deposited from solution in high density (Supporting Information, Figure S3) to form a thin-film there is no preferred axial orientation of the nanorods in the final layer (given the random packing of the ANCs). As resolute vertical alignment of nanorods in a thin-film is attractive for absorber layers, we investigated cluster deassembly in solution for subsequent reassembly at a substrate interface. This was achieved using partial ligand exchange with oleylamine where a rapid solution transformation from opaque to translucent occurred upon addition (Supporting Information, Figure S4a). DLS measurements confirmed the cluster deassembly with the hydrodynamic radius of ~25 nm consistent with the length of a discrete nanorod (Supporting Information, Figure S4b). Fourier transform infrared spectroscopy (FTIR) confirmed the partial ligand exchange where in addition to the characteristic S−H vibration peak at 2570 cm^{-1} (from the thiol), the antisymmetric and symmetric vibration modes of −N−H are observed between 3300 and 3500 cm^{-1} with NH_2 scissoring modes at 1570 cm^{-1} (Supporting Information, Figure S5a).[34] The survey XPS spectra of as-synthesized CIGS nanorods (Supporting Information, Figure S5b) show the presence of Cu, In, Ga, S, O, C, with N detected after ligand exchange. The high resolution spectra of S 2p

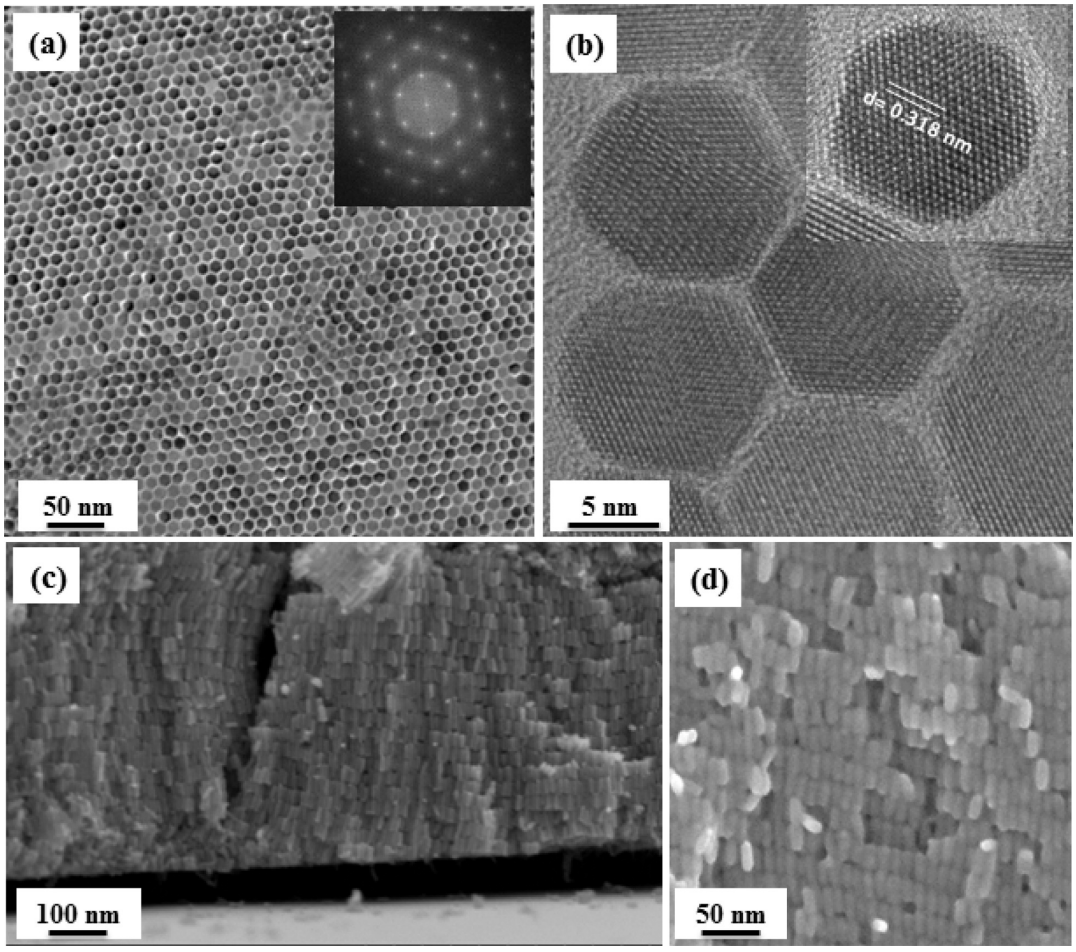

Figure 4. (a) Top down TEM image of monolayer sheet of vertically assembled CIGS nanorods with inset FFT pattern. (b) TEM images showing the closed-packed 2D superlattice with inset HRTEM image of single nanorod. (c) SEM cross-section image shows the multilayered assembly of nanorods. During sample cleaving, the multilayer nanorod film has delaminated resulting in the dark feature between the layer and substrate. (d) High-resolution SEM image shows the vertically alignment of CIGS nanorods.

(Figure 3b) from the as-synthesized CIGS nanorods can be fitted well with two spin−orbit doublets of intensity ratio 1:2 for $2p_{1/2}$: $2p_{3/2}$ and doublet separation of 1.2 eV. The doublet with S $2p_{3/2}$ peak at 161.7 eV is attributed to sulphide ions of the nanorods.[40] The second doublet at 162.7 eV can be assigned to thiolate sulfur bonded to the nanorod surface.[41] The S 2p spectrum from the ligand exchanged nanorods (Figure 3c) can be fitted in a similar manner yielding a relatively low fraction of thiolate sulfur which is expected as the amine displaces thiols forming stronger bonds with the surface atoms. An additional broad peak at ~169 eV is attributed to oxidized sulfur in the form of Sulphone or sulfate species. The related N 1s spectrum of the amine exchanged CIGS (Figure 3d) shows the presence of nitrogen in two different chemical states. The peak at 399.3 eV corresponds to neutral C−N bonding in amine and the prominent shoulder at higher binding energy of 401.3 eV to positively charged nitrogen (C−N+) resulting from coordination of the N in the amine to the metal ions.[42]

The thiol/amine capped nanorods did not undergo spontaneous supercrystallization regardless of time. In contrast, thiol/amine capped nanorods only self-assemble at an optimal concentration, forming 2D superstructures which drop to the surface under gravity sedimentation correlating with the charge/dipole-based mechanism previously reported.[21−23] Figure 4a shows low-resolution TEM images of a monolayer of vertically aligned thiol/amine capped CIGS nanorods that self-assemble at an optimal concentration of (5×10^{-5} molL^{-1}). The inset FFT pattern demonstrates the resolute hexagonal ordering. Further magnified HRTEM images are shown in Figure 4b with the inset top-down HRTEM image of a single nanorod showing the *d*-spacing in the lattice fringes is 0.318 nm, which matches with the (002) plane of wurtzite structure. The influence of charge and dipole can be further utilized to achieve perpendicular assembly over large (device scale areas) using electrophoresis. Here the charge ensures field driven migration whereas the dipole ensures orientational order in the deposit. Using a field strength of 150−200 V, highly ordered deposits over

device scale areas and over several multilayers were obtained (Figure 4c). The further HRSEM image in Figure 4d shows that the nanorods are vertical oriented in all the layers.

The greater ζ potential of the thiol/amine capped nanorods, ~33 ± 4 mV, to that of the thiol capped nanorods, ~7 ± 3 mV, (Supporting Information, Figure S6) significantly impacts their respective assembly protocols. The thiol/amine capped nanorods have large columbic repulsion in solution which maintains the dispersion such that no assembly is occurring outside of an optimized concentration. The 2D assembly of thiol/amine capped nanorods in solution therefore follows the expected lowest energy consideration with a distance (concentration) dependence that balances attractive and repulsive interactions for assembly. In contrast, for the thiol capped nanorods, dipole−dipole forces are much stronger as the columbic repulsion is less prominent. The spontaneous clustering of the thiol capped nanorods at low dilution for the formation of 3D assemblies clearly occurs by a different mechanism. The time dependence (3−4 h) suggests that this assembly is predominantly entropy driven where the free energy of the system increases when solute molecules are eliminated from between the nanorods. For supracrystals to form the nanorods need to find their preferred place on the growing crystal structure before locking in, resulting in the most energetically stable configuration (3D *versus* 2D) yielding the greatest entropy gain.[43−48] Clearly other interparticle interactions cannot be discounted. van der Waals studies in nanorods have shown the length of the ligand will predicate the preference for end-to-end or side-to-side assembly (or both) with shorter lengths increasing the propensity for end-to-end.[43] Here the thiols are shorter than the oleylamine in good agreement with the simultaneous occurrence of end-to-end and side-to-side. In support of this, if thiol capped nanorods are rapidly assembled from an evaporated solvent before clustering occurs, end-to-end patterns form in preference to side-by-side (Figure 5a,b).

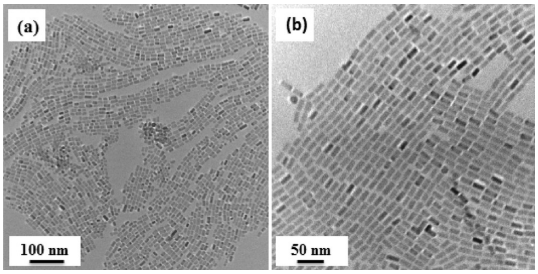

Figure 5. (a,b) Low and high-resolution TEM images show end-to-end assembly of nanorods.

CONCLUSIONS

In summary, the reversible assembly and disassembly of CIGS nanorods is demonstrated over two and three dimensions from solution. This approach is generally applicable to copper chalcogenide nanorods synthesized with thiol ligands (see comparable assemblies demonstrated with ternary $CuInS_2$ nanorods: Supporting Information, Figure S7). We show that the assembly protocol is dictated by the ligand environment and is hence chemically tunable. This approach allows the collective properties of CIGS nanorods to be harnessed either as micrometer sized clusters, or in monolayer and multilayer assemblies extending over device scale areas. The density of packing, perpendicular order, and evidence of absorption enhancement in the assemblies make these structures highly attractive for scalable application in photovoltaic devices.

METHODS

Materials. All reagents were used as received without any further purification. Copper(II) acetylacetonate ($Cu(acac)_2$, 99.99%), indium(III) acetylacetonate ($In(acac)_3$, 99.99%), gallium(III) acetylacetonate ($Ga(acac)_3$, 99.99%), 1-dodecanethiol (1-DDT, >97%), *tert*-dodecanethiol (*t*-DDT, 98.5%, mixture of isomers), oleylamine (OLA, 70%, technical grade) and 1-octadecene (ODE, 90%, technical grade) were purchased from Aldrich. Trioctylphosphine oxide (TOPO, 99%) was purchased from Strem Chemicals.

Synthesis of $CuIn_{0.75}Ga_{0.25}S_2$ (CIGS) Nanorod. CIGS nanorods were synthesized using a modification of a previously published procedure.[1] For a typical synthesis of CIGS nanocrystals, $Cu(acac)_2$ (0.2618 g, 1 mmol), $In(acac)_3$ (0.3091 g, 0.75 mmol), $Ga(acac)_3$ (0.0918 g, 0.25 mmol), and TOPO (1.3532 g, 3.5 mmol) were mixed with 10 mL of 1-octadecene in a three-neck round-bottom flask and evacuated at room temperature for 30 min. The solution was then heated to 250−270 °C in 15−20 min under an argon atmosphere. At 155 °C, a mixture of 0.5 mL of 1-DDT and 1.5 mL of *t*-DDT was injected into the flask which resulted in an immediate color change from dark green to light yellow. After injection, the reaction was allowed to proceed for 10−15 min with continuous stirring. Subsequently, the heating mantle was removed and the reaction vessel was allowed to cool to 80 °C. A 2−3 mL portion of anhydrous toluene was added initially to quench the reaction. The nanorods were then washed in a 2:1 ratio of toluene to ethanol and centrifuged at 4000 rpm for 10 min to yield a dark-red centrifuged product. The key step for synthesis of monodispersed CIGS nanorod is the increase in 1-DDT concentration in the reaction and growth time for the nanorod formation, as 1-DDT binds more strongly to facets other than the (002) allowing nanorod growth in this direction.

Ligand Exchange. For ligand exchange, 100 μL of oleylamine is carefully added to 5 mL of toluene solution of as-synthesized CIGS/CIS nanorods. With the addition of amine solution an immediate change in the dispersion of the nanorods solution is visualized. Further, the resulting solution was sonicated for 10 min in the sonication bath. The solution was washed with 1:1 ratio of toluene and ethanol and centrifuged at 4000 rpm for 5 min and the supernatant was discarded. An important extra care was taken during ligand exchange; the oleylamine capped nanocrystal were washed 3−5 time with nonsolvent (ethanol, methanol) to remove any excess oleylamine in the nanocrystal solution, as nanocrystal shows etching behavior over the time in the presence of excess oleylamine (images not shown here). Similar behavior of the etching of nanocrystal due to excess oleylamine was previously seen on $CuInSe_2$.[49,50]

Monolayer Assembly of Nanorods. The self-assembly of CIGS and CIS nanorods was undertaken by dropcasting the nanorod solution with various concentrations ranging from 10^{-8} to 10^{-2} mol L^{-1} on to a carbon supported Cu-TEM grids. The solvent was allowed to evaporate slowly under a constant evaporation rate (in an argon glovebox, with 0% relative humidity). The optimum concentration for vertical assembly was found to be 5×10^{-5} mol L^{-1}. The strict concentration dependence of nanorods solution is typical for perpendicular nanorod assembly where outside of a certain window randomly deposited nanorods are found on the substrate.

Multilayer Assembly of Nanorods by Electrophoresis. A toluene solution of CIGS nanorods (10% w/v) was used for electrophoresis. During electrophoresis, the silicon substrates (10 mm × 10 mm) were attached onto the negative electrode of two parallel gold-coated copper electrodes which are separated at 2 mm apart. The electrodes were completely immersed in a nanorod solution, and a potential of 150−200 V was applied to the substrate for 3 min using a high voltage power supply unit (TECHNIX SR-5-F-300, S/N: BU08/04971). Voltage was monitored using a Black star 3225 MP millimeter.

Electron Microscopy. The CIGS/CIS nanorods and their assemblies were characterized by transmission electron microscopy (TEM), angular dark-field scanning transmission electron microscopy by using a JEOL JEM-2011F operating at an accelerating voltage of 200 kV. High resolution scanning electron microscopy (SEM) of the nanorods assembly on a Si (111) substrate was performed by a Hitachi SU-70 machine.

X-ray Diffraction Analysis. The sample for X-ray diffractograms analysis was prepared by drop-casting the nanorod solution on a glass substrate. The analysis was carried out on a PANalytical X'Pert MPD Pro using Cu Kα radiation with a 1-D X'Celerator strip detector.

UV−vis Absorption Spectroscopy. UV−vis spectroscopy of the nanorod solutions was performed on a PerkinElmer's LAMBDA 45 and 35 UV−vis spectrophotometer operated at a resolution of 1 nm.

Fourier Transform Infrared Spectroscopy. All spectra were taken in transmission mode on a model Perkin-Elmer-Spectrum at a spectral resolution of 4 cm^{-1}. FTIR measurements were carried out for the nanorod solution drop casted on Si or glass substrates.

X-ray Photoelectron Spectroscopy. XPS measurement of the as-synthesized and ligand-exchanged CIGS nanorods were carried out using a Kratos Axis 165 spectrometer. High resolution spectra were taken using monochromated Al Kα radiation of energy of 1486.6 eV at fixed pass energy of 20 eV. For peak synthesis, a mixed Gaussian-Lorenzian function with a Shirley-type background subtraction was used. Samples were flooded with low energy electrons for efficient charge neutralization. Binding energies (BE) were determined using C 1s at 284.8 eV as charge reference.

Dynamic Light Scattering. The size of CIGS and CIS ANCs was measured by Dynamic Light Scattering (DLS) using Zetasizer Nano ZS DLS system (Malvern Instruments Ltd., England). The laser specifications for this Zetasizer were 4mW He or Ne laser with a 633 nm wavelength. DTS applications 5.10 software was used to analyze the data. For each sample, four DLS measurements were conducted with a number of runs.

Conflict of Interest: The authors declare no competing financial interest.

Acknowledgment. This work was supported by Science Foundation Ireland (SFI) under the Principal Investigator Program under contract No. 11PI-1148 and also by the Advanced Biomimetic Materials for Solar Energy Conversion Strategic Research Cluster (Contract 07/SRC/B1160). The authors acknowledge Joseph A. Murphy and Amita Joshi for Zeta Potential and DLS measurement.

Supporting Information Available: Synthesis of $CuInS_2$ nanorods, DLS size distributions, graph of assembled and deassembled CIGS ANCs; Tauc plot of CIGS nanorods, zeta-potential measurement, FTIR spectra of CIGS ANCs after partial ligand exchange with oleylamine, XPS survey spectra of CIGS nanorods before and after ligand exchange; SEM and TEM image of ANCs of $CuInS_2$ nanorods. This material is available free of charge *via* the Internet at http://pubs.acs.org.

REFERENCES AND NOTES

1. Habas, S. E.; Platt, H. A. S; van Hest, M. F. A. M; Ginley, D. S. Low-Cost Inorganic Solar Cells: From Ink to Printed Device. *Chem. Rev.* **2010**, *110*, 6571–6594.
2. van Hest, M. F. A. M.; Ginley, D. S. Future Directions for Solution-Based Processing of Inorganic Materials. In *Solution Processing of Inorganic Materials*; Mitzi, D. B., Ed.; Wiley: Hoboken, NJ, 2008.
3. Guo, Q.; Ford, G. M.; Hillhouse, H. W.; Agrawal, R. Sulfide Nanocrystal Inks for Dense $Cu(In_{1-x}Ga_x)(S_{1-y}Se_y)_2$ Absorber Films and Their Photovoltaic Performance. *Nano Lett.* **2009**, *9*, 3060–3065.
4. Panthani, M. G.; Akhavan, V.; Goodfellow, B.; Schmidtke, J. P.; Dunn, L.; Dodabalapur, A.; Barbara, P. F.; Korgel, B. A. Synthesis of $CuInS_2$, $CuInSe_2$, and $Cu(In_xGa_{1-x})Se_2$ (CIGS) Nanocrystal "Inks" for Printable Photovoltaics. *J. Am. Chem. Soc.* **2008**, *130*, 16770–16777.
5. Chang, S.-H.; Chiang, M.-Y.; Chiang, C.-C.; Yuan, F.-W.; Chen, C.-Y.; Chiu, B.-C.; Kao, T.-L.; Lai, C.-H.; Tuan, H.-Y. Facile Colloidal Synthesis of Quinary $CuIn_{1-x}Ga_x(S_ySe_{1-y})_2$ (CIGSSe) Nanocrystal Inks with Tunable Band Gaps for use in Low-Cost Photovoltaics. *Energy Environ. Sci.* **2011**, *4*, 4929–4932.
6. Zhong, H.; Lo, S. S.; Mirkovic, T.; Li, Y.; Ding, Y.; Li, Y.; Scholes, G. D. Noninjection Gram-Scale Synthesis of Monodisperse Pyramidal $CuInS_2$ Nanocrystals and Their Size-Dependent Properties. *ACS Nano* **2010**, *4*, 5253–5262.
7. Cao, Q.; Gunawan, O.; Copel, M.; Reuter, K. B.; Chey, S. J.; Deline, V. R.; Mitzi, D. B. Defects in $Cu(In,Ga)Se_2$ Chalcopyrite Semiconductors: A Comparative Study of Material Properties, Defect States, and Photovoltaic Performance. *Adv. Energy Mater.* **2011**, *1*, 845–853.
8. Wang, D.; Wan, L.; Bai, Z.; Cao, Y. Mixed Phases in p-type $CuInSe_2$ Thin Films Detected by Using Micro-Raman Scattering Spectroscopy. *Appl. Phys. Lett.* **2008**, *92*, 211912.
9. Ras, D. A-.; Schaffer, B.; Schaffer, M.; Schmidt, S. S.; Caballero, R.; Unold, T. Direct Insight into Grain Boundary Reconstruction in Polycrystalline $Cu(In,Ga)Se_2$ with Atomic Resolution. *Phys. Rev. Lett.* **2012**, *108*, 075502.
10. Chen, X.; Shen, S.; Guo, L.; Mao, S. S. Semiconductor-Based Photocatalytic Hydrogen Generation. *Chem. Rev.* **2010**, *110*, 6503–6570.
11. Ibáñez, M.; Cadavid, D.; Zamani, R.; Garca-Castello, N.; Izquierdo-Roca, V.; Li, W.; Fairbrother, A.; Prades, J. D.; Shavel, A.; Arbiol, J.; *et al.* $Cu_2ZnGeSe_4$ Nanocrystals: Synthesis and Thermoelectric Properties. *Chem. Mater.* **2012**, *24*, 562–570.
12. Todorov, T. K.; Gunawan, O.; Gokmen, T.; Mitzi, D. B. Solution-Processed $Cu(In,Ga)(S,Se)_2$ Absorber Yielding a 15.2% Efficient Solar Cell. *Prog. Photovolt: Res. Appl.* **2012**, 10.1002/pip.1253.
13. Kruszynska, M.; Borchert, H.; Parisi, J.; Kolny-Olesiak, J. Synthesis and Shape Control of $CuInS_2$ Nanoparticles. *J. Am. Chem. Soc.* **2010**, *132*, 15976–15986.
14. Wang, Y.-H. A.; Zhang, X.; Bao, N.; Lin, B.; Gupta, A. Synthesis of Shape-Controlled Monodisperse Wurtzite $CuIn_xGa_{1-x}S_2$ Semiconductor Nanocrystals with Tunable Band Gap. *J. Am. Chem. Soc.* **2011**, *133*, 11072–11075.
15. Singh, A.; Geaney, H.; Laffir, F.; Ryan, K. M. Colloidal Synthesis of Wurtzite Cu_2ZnSnS_4 Nanorods and Their Perpendicular Assembly. *J. Am. Chem. Soc.* **2012**, *134*, 2910–2913.
16. Lu, X.; Zhuang, Z.; Peng, Q.; Li, Y. Controlled Synthesis of Wurtzite $CuInS_2$ Nanocrystals and Their Side-by-Side Nanorod Assemblies. *CrystEngComm* **2011**, *13*, 4039–4045.
17. Hu, J.; Li, L.-S.; Yang, W.; Manna, L.; Wang, L.-W.; Alivisatos, A. P. Linearly Polarized Emission from Colloidal Semiconductor Quantum Rods. *Science* **2001**, *292*, 2060–2063.

18. Krahne, R.; Morello, G.; Figuerola, A.; George, C.; Deka, S.; Manna, L. Physical Properties of Elongated Inorganic Nanoparticles. *Phys. Rep* **2011**, *501*, 75–221.
19. Gonzalez-Valls, I.; Lira-Cantu, M. Vertically-Aligned Nanostructures of ZnO for Excitonic Solar Cells: A Review. *Energy Environ. Sci.* **2009**, *2*, 19–34.
20. Liu, K.; Zhao, N. N.; Kumacheva, E. Self-Assembly of Inorganic Nanorods. *Chem. Soc. Rev.* **2010**, *40*, 656–671.
21. Singh, A.; Gunning, R. D.; Sanyal, A.; Ryan, K. M. Directing Semiconductor Nanorod Assembly into 1D or 2D Supercrystals by Altering the Surface Charge. *Chem. Commun.* **2010**, *46*, 7193–7195.
22. Singh, A.; Gunning, R. D.; Ahmed, S.; Barrett, C. A.; English, N. J.; Garate, J.-A.; Ryan, K. M. Controlled Semiconductor Nanorod Assembly from Solution: Influence of Concentration, Charge and Solvent Nature. *J. Mater. Chem.* **2012**, *22*, 1562–1569.
23. Singh, A.; Dickinson, C.; Ryan, K. M. Insight into the 3D Architecture and Quasicrystal Symmetry of Multilayer Nanorod Assemblies from Moiré Interference Patterns. *ACS Nano* **2012**, *6*, 3339–3345.
24. Baranov, D.; Fiore, A.; van Huis, M.; Giannini, C.; Falqui, A.; Lafont, U.; Zandbergen, H.; Zanella, M.; Cingolani, R.; Manna, L. Assembly of Colloidal Semiconductor Nanorods in Solution by Depletion Attraction. *Nano Lett.* **2010**, *10*, 743–749.
25. Baker, J. L.; Widmer-Cooper, A.; Toney, M. F.; Geissler, P. L.; Alivisatos, A. P. Device-Scale Perpendicular Alignment of Colloidal Nanorods. *Nano Lett.* **2010**, *10*, 195–201.
26. Zanella, M.; Gomes, R.; Povia, M.; Giannini, C.; Zhang, Y.; Riskin, A.; van Bael, M.; Hens, Z.; Manna, L. Self-Assembled Multilayers of Vertically Aligned Semiconductor Nanorods on Device-Scale Areas. *Adv. Mater.* **2011**, *23*, 2205–2209.
27. Rivest, J. B.; Swisher, S. L.; Fong, L.-K.; Zheng, H.; Alivisatos, A. P. Assembled Monolayer Nanorod Heterojunctions. *ACS Nano* **2011**, *5*, 3811–3816.
28. Ahmed, S.; Ryan, K. M. Centimetre Scale Assembly of Vertically Aligned and Close Packed Semiconductor Nanorods from Solution. *Chem. Commun.* **2009**, 6421–6423.
29. Kelly, D.; Singh, A.; Barrett, C. A.; O'Sullivan, C.; Coughlan, C.; Laffir, F. R.; O'Dwyer, C.; Ryan, K. M. A Facile Spin-Cast Route for Cation Exchange of Multilayer Perpendicularly-Aligned Nanorod Assemblies. *Nanoscale* **2011**, *3*, 4580–4583.
30. Ahmed, S.; Ryan, K. M. Self-Assembly of Vertically Aligned Nanorod Supercrystals Using Highly Oriented Pyrolytic Graphite. *Nano Lett.* **2007**, *7*, 2480–2485.
31. Ryan, K. M.; Mastroianni, A.; Stancil, K. A.; Liu, H. T.; Alivisatos, A. P. Electric-Field-Assisted Assembly of Perpendicularly Oriented Nanorod Superlattices. *Nano Lett.* **2006**, *6*, 1479–1482.
32. Carbone, L.; Nobile, C.; De Giorgi, M.; Della Sala, F.; Morello, G.; Pompa, P.; Hytch, M.; Snoeck, E.; Fiore, A.; Franchini, I. R.; *et al.* Synthesis and Micrometer-Scale Assembly of Colloidal CdSe/CdS Nanorods Prepared by a Seeded Growth Approach. *Nano Lett.* **2007**, *7*, 2942–2950.
33. Kriegel, I.; Rodriguez-Fernandez, J.; Como, E. D.; Lutich, A. A.; Szeifert, J. M.; Feldmann, J. Tuning the Light Absorption of $Cu_{1.97}S$ Nanocrystals in Supercrystal Structures. *Chem. Mater.* **2011**, *23*, 1830–1834.
34. Zhuang, Z.; Peng, Q.; Zhang, B.; Li, Y. Controllable Synthesis of Cu_2S Nanocrystals and Their Assembly into a Superlattice. *J. Am. Chem. Soc.* **2008**, *130*, 10482–10483.
35. Talapin, D. V.; Lee, J. S.; Kovalenko, M. V.; Shevchenko, E. V. Prospects of Colloidal Nanocrystals for Electronic and Optoelectronic Applications. *Chem. Rev.* **2010**, *110*, 389–458.
36. Quan, Z. W.; Fang, J. Y. Superlattices with Non-spherical Building Blocks. *Nano Today* **2010**, *5*, 390–411.
37. West, A. *Basic Solid State Chemistry*, 2nd ed.; John Wiley & Sons: Chichester, 1999.
38. Wang, J.-J.; Xue, D.-J.; Guo, Y.-G.; Hu, J.-S.; Wan, L.-J. Bandgap Engineering of Monodispersed $Cu_{2-x}S_ySe_{1-y}$ Nanocrystals through Chalcogen Ratio and Crystal Structure. *J. Am. Chem. Soc.* **2011**, *133*, 18558–18561.
39. Kriegel, I.; Jiang, C.; Rodríguez-Fernández, J.; Schaller, R. D.; Talapin, D. V.; da Como, E.; Feldmann, J. Tuning the Excitonic and Plasmonic Properties of Copper Chalcogenide Nanocrystals. *J. Am. Chem. Soc.* **2012**, *134*, 1583–1590.
40. NIST-XPS database, version 3.5 (http://srdata.nist.gov/xps/). Accessed 12/03/2012.
41. Loepp, G.; Vollmer, S.; Witte, G.; Wöll, Ch. Adsorption of Heptanethiol on Cu(110). *Langmuir* **1999**, *15*, 3767–3772.
42. Kowalski, D.; Schmuki, P. Polypyrrole Self-Organized Nanopore Arrays Formed by Controlled Electropolymerization in TiO_2 Nanotube Template. *Chem. Commun.* **2010**, *46*, 8585–8587.
43. Bishop, K. J. M.; Wilmer, C. E.; Soh, S.; Grzybowski, B. A. Nanoscale Forces and Their Uses in Self-Assembly. *Small* **2009**, *5*, 1600–1630.
44. Evers, W. H.; De Nijs, B.; Filion, L.; Castillo, S.; Dijkstra, M.; Vanmaekelbergh, D. Entropy-Driven Formation of Binary Semiconductor-Nanocrystal Superlattices. *Nano Lett.* **2010**, *10*, 4235–4241.
45. Bodnarchuk, M. I.; Kovalenko, M. V.; Heiss, W.; Talapin, D. V. Energetic and Entropic Contributions to Self-Assembly of Binary Nanocrystal Superlattices: Temperature as the Structure Directing Factor. *J. Am. Chem. Soc.* **2010**, *132*, 11967–11977.
46. Miszta, K.; Graaf, J.; de; Bertoni, G.; Dorfs, D.; Brescia, R.; Marras, S.; Ceseracciu, L.; Cingolani, R.; Roij, R. va.; Dijkstra, M.; *et al.* Hierarchical Self-Assembly of Suspended Branched Colloidal Nanocrystals into Superlattice Structures. *Nat. Mater.* **2011**, *10*, 872–876.
47. Talapin, D. V.; Shevchenko, E. V.; Murray, C. B.; Kornowski, A.; Förster, S.; Weller, H. CdSe and CdSe/CdS Nanorod Solids. *J. Am. Chem. Soc.* **2004**, *126*, 12984–12988.
48. Zhuang, Z. B.; Peng, Q.; Wang, X.; Li, Y. D. Tetrahedral Colloidal Crystals of Ag_2S Nanocrystals. *Angew. Chem., Int. Ed.* **2007**, *46*, 8174–8177.
49. Koo, B.; Patel, R. N.; Korgel, B. A. Synthesis of $CuInSe_2$ Nanocrystals with Trigonal Pyramidal Shape. *J. Am. Chem. Soc.* **2009**, *131*, 3134–3135.
50. Allen, P. M.; Bawendi, M. G. Ternary I–III–VI Quantum Dots Luminescent in the Red to Near-infrared. *J. Am. Chem. Soc.* **2008**, *130*, 9240–9241.